Two-stage Perimeter Signal Control with Spillback-aware Set-points based on Network Buffer Capacity

Zilin Shen[1,2], Zicheng Su*[2], Chunhui Yu[2], and Wanjing Ma*[2]

[1]Urban Mobility Institute, Tongji University, 4800 Cao'an Road, Shanghai 201804, China
[2]The Key Laboratory of Road and Traffic Engineering of the Ministry of Education, Tongji University, 4800 Cao'an Road, Shanghai 201804, China

Short summary

Managing cordon queues and spillback is one of the major challenges in perimeter control (PC). To address this issue, this study proposes a two-stage framework for signal optimization at perimeter intersections. In Stage I, the concept of network buffer capacity is introduced, together with a calibration method. Based on this concept, the optimal gated inflows are determined through a spillback-aware multi-objective model to jointly account for network- and cordon-level control objectives. The weight coefficients in the model are adaptively adjusted according to the real-time traffic states. In Stage II, the green durations and phase structures of each perimeter intersection are simultaneously optimized using a group-based signal control approach. Experiments show that, compared with traditional feedback PC strategies, the proposed framework significantly mitigates cordon spillback while preventing network gridlock. The results also highlight the necessity of jointly optimizing phase structures and green durations under time-varying traffic conditions.
Keywords: Perimeter control, two-stage optimization, network buffer capacity, group-based signal control

1 Introduction

Traffic signal control is essential for mitigating urban congestion and improving travel efficiency. While isolated intersection and arterial control methods can enhance local performance, they are insufficient under oversaturated conditions and may lead to network gridlock. Perimeter control (PC) has therefore been developed as a network-level gating strategy to regulate inflow into a protected network (PN), typically based on the macroscopic fundamental diagram (MFD), whose empirical validity has been widely demonstrated (Geroliminis & Daganzo, 2008). Various PC strategies have been proposed, including PI-based feedback control (Keyvan-Ekbatani et al., 2012), model predictive control (MPC) (Geroliminis et al., 2012), and data-driven approaches (Chen et al., 2022), aiming to maintain the network state within the efficient operating regime.

Despite these advances, most existing PC studies primarily determine total gated inflow from a network-level perspective, overlooking the cordon-level performance. This may lead to cordon spillback and disrupt traffic outside the PN. To address this issue, some studies incorporate boundary queues into perimeter control models (Haddad, 2017), while others attempt to mitigate spillback by balancing queue lengths using optimization models (Keyvan-Ekbatani et al., 2021) or learning-based frameworks (Ni & Cassidy, 2019). In addition, dynamic perimeter approaches have been proposed to adjust the network boundary over time (Hamedmoghadam et al., 2022). However, these methods either treat cordon queue as a secondary effect or introduce additional uncertainties to adjacent regions. As a result, a systematic mechanism is still lacking to explicitly manage the trade-off between network-level efficiency and cordon-level queue management under a fixed cordon area.

Several studies adopt multi-objective formulations to account for the balance between network throughput and cordon performance. For example, MPC-based approaches incorporate both network-level and cordon-level objectives into the control framework (Yang et al., 2017), while PI-based methods introduce additional objectives to regulate boundary queues (Tsitsokas et al., 2023). However, these approaches typically rely on pre-defined and fixed weights, without explicitly characterizing the real-time spillback risk, limiting their responsiveness to the time-varying

traffic conditions. Other frameworks, such as Max Pressure-based or reinforcement learning-based methods, improve empirical performance but do not provide clear theoretical insights into the trade-off mechanism (Liu & Gayah, 2024; Yu et al., 2025). The conditions under which cordon spillback can be prevented while preventing network gridlock remain insufficiently understood.

Another limitation lies in the implementation of signal timings at perimeter intersections. Most existing approaches focus on adjusting the green durations of gated movements, with limited attention to phase structures. Although some studies consider optimizing green splits for all movements (Keyvan-Ekbatani et al., 2019), the sequence and combination of gated and non-gated movements are typically fixed. Considering that time-varying and asymmetric demand patterns under PC strategies often arise due to feedback regulation (Keyvan-Ekbatani et al., 2021), such rigid signal settings can lead to suboptimal control performance, weakening the effectiveness of perimeter control.

To address these limitations, this study proposes a two-stage optimization framework. The first stage introduces the concept of network buffer capacity and develops a spillback-aware multi-objective model to determine optimal gated inflows. The second stage optimizes both green durations and phase structures under a group-based signal control framework, enabling adaptive coordination between gated and non-gated movements. The effectiveness of the proposed framework is validated through microscopic traffic simulations.

2 Methodology

Calibration of buffer capacity

Extensive studies have shown that urban networks can operate stably when accumulation is maintained within a certain range around the critical accumulation of the MFD curve (Daganzo, 2007; Ambühl et al., 2020). Based on this property, we introduce the concept of *buffer capacity*, defined as the additional number of vehicles that PN can accommodate beyond the critical accumulation N^{cr} without causing network gridlock. To quantify this capacity, we adopt the trapezoidal MFD formulation proposed in Daganzo et al. (2018), as shown in Figure 1. The shape is determined by the key traffic parameters $[v_f, w, F_{\max}, N^{\text{jam}}]$, where v_f denotes the free-flow speed, w the backward wave speed, $F_{\max}$ the maximum weighted average flow, and N^{jam} the accumulation at jam density. The trapezoidal MFD can be formulated by:

$$F_{up}(N) = \begin{cases} v_f N, & N \le N^{lb}; \\ F_{\max}, & N^{lb} < N \le N^{ub}; \\ w(N^{\text{jam}} - N), & N > N^{ub}. \end{cases} \tag{1}$$

where N^{lb} and N^{ub} denote the minimum and maximum accumulation of the flat-peak region of the trapezoidal MFD, respectively.

To better fit real-world data, Ambühl et al. (2020) proposed a smooth approximation of the trapezoidal MFD, namely, the λ-trapezoidal MFD, whose functional form is given by:

$$F(N) = -\lambda \ln\left(e^{-\frac{v_f N}{\lambda}} + e^{-\frac{F_{\max}}{\lambda}} + e^{-\frac{w(N^{\text{jam}} - N)}{\lambda}}\right) \tag{2}$$

where λ is the smoothing parameter, which describes the gap between the trapezoidal MFD and the empirical MFD caused by microscopic traffic behaviors (Ambühl et al., 2020).

To calibrate the parameters in Eq. (2), a two-stage fitting procedure is applied. First, the trapezoidal MFD parameters $[v_f, w, F_{\max}, N^{\text{jam}}]$ are estimated. Then, λ is calibrated with the above parameters fixed (Ma et al., 2024). Once these parameters are obtained, N^{ub} can be derived by:

$$N^{ub} = N^{\text{jam}} - \frac{F_{\max}}{w} \tag{3}$$

The buffer capacity of the PN is then quantified as the difference between N^{ub} and N^{cr}. This margin can be exploited to balance network-level and cordon-level performance, allowing a moderate increase in network accumulation to alleviate excessive cordon queues.

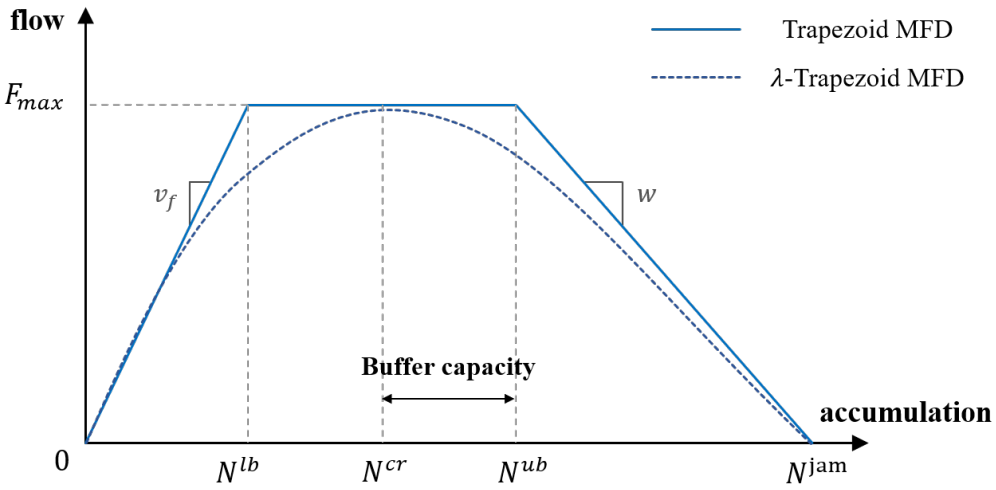


Figure 1: An illustration of buffer capacity.

Stage I: Centralized optimization of gated inflow

The proportional-integral (PI) feedback regulator has been widely adopted in perimeter control because of its simplicity, robustness, and real-time applicability (Keyvan-Ekbatani et al., 2012; Kouvelas et al., 2017). Under the PI regulator, the total gated inflow can be calculated by:

$$u^{cr}(k) = u(k-1) - K_{\mathrm{P}}\left(N(k) - N(k-1)\right) + K_{\mathrm{I}}\left(N^{cr} - N(k)\right) \tag{4}$$

where u^{cr} is the total inflow corresponding to N^{cr}; $u(k-1)$ denotes the actual total inflow in the last interval; $N(k)$ and $N(k-1)$ are the PN accumulation at intervals k and $k-1$, respectively; K_{P} and K_{I} are the proportional and integral gains.

In this study, we define u^{cr} as *critical total inflow*, which maintains the network accumulation around N^{cr}. In most existing studies, u^{cr} is directly treated as the desired total inflow and then distributed among gated links. Although this strategy is effective for preserving network-level efficiency, it does not explicitly account for cordon-level queue accumulation and spillback at perimeter intersections. Consequently, external congestion may propagate outside the PN.

To incorporate spillback prevention into the PC framework, we introduce the concept of *increased total inflow*, denoted by u^{ir}, based on the buffer capacity. Specifically, u^{ir} is obtained by replacing N^{cr} with N^{ub} in Eq. (4), yielding:

$$u^{ir}(k) = u(k-1) - K_{\mathrm{P}}\left(N(k) - N(k-1)\right) + K_{\mathrm{I}}\left(N^{ub} - N(k)\right) \tag{5}$$

Together, u^{cr} and u^{ir} define an effective operating range for the total gated inflow, within which the accumulation of the PN remains in the flat-peak region of the trapezoidal MFD. Accordingly, Stage I formulates a centralized multi-objective optimization model (named *PI-Balance* or PIB for short) to determine the distributed gated inflow:

P1:

$$\min_{\mathbf{u}} J = \left(\sum_{i\in\mathcal{I}}\sum_{p\in\mathcal{P}_i^{\text{in}}} u_{i,p}(k) - u^{cr}(k)\right)^2 + \sum_{i\in\mathcal{I}}\sum_{p\in\mathcal{P}_i^{\text{in}}} \omega_{i,p}(k) q_{i,p}(k+1)^2 \tag{6}$$

$$\text{subject to} \quad q_{i,p}(k+1) = q_{i,p}(k) + a_{i,p}(k)C - u_{i,p}(k), \qquad \forall i\in\mathcal{I}, p\in\mathcal{P}_i^{\text{in}} \tag{7}$$

$$u_{i,p}^{\min} \le u_{i,p}(k) \le u_{i,p}^{\max}, \qquad \forall i\in\mathcal{I}, p\in\mathcal{P}_i^{\text{in}} \tag{8}$$

$$u_{i,p}(k) \le c_{i,p}^{down} - q_{i,p}^{down}(k), \qquad \forall i\in\mathcal{I}, p\in\mathcal{P}_i^{\text{in}} \tag{9}$$

$$\sum_{i\in\mathcal{I}}\sum_{p\in\mathcal{P}_i^{\text{in}}} u_{i,p}(k) \le u^{ir}(k) \tag{10}$$

where $q_{i,p}(k)$ and $a_{i,p}(k)$ denote the initial queue length and the arrival rate of lane group (i,p) at interval k, respectively; C the common cycle length of all perimeter intersections; $u_{i,p}^{\min}$ and

$u_{i,p}^{\max}$ the minimum and maximum inflow; $c_{i,p}^{down}$ and $q_{i,p}^{down}(k)$ the capacity and queue length of the downstream lane group of lane group (i,p), respectively.

It should be noted that in this study, the optimization unit is a *lane group*, defined as a set of lanes on the same approach that share a common green phase. The tuple (i,p) denotes lane group p at intersection i, where $i \in \mathcal{I}$ and $p \in \mathcal{P}_i$. Here, $\mathcal{I}$ is the set of perimeter intersections, and $\mathcal{P}_i$ is the set of lane groups at intersection i. Specifically, $\mathcal{P}_i^{\text{in}}$ and $\mathcal{P}_i^{\text{out}}$ denote the gated lane groups that discharge flow into the PN and out of the PN, respectively. The benefit of using lane groups as the optimization unit is that it enables more flexible coordination of gated and non-gated movements at perimeter intersections.

The objective function consists of two components representing network-level and cordon-level control objectives, respectively. The first term minimizes the deviation between the total gated inflow and the critical total inflow $u^{cr}(k)$, thereby keeping the operational efficiency of the PN. The second term minimizes the weighted sum of squared queue lengths of all gated lane groups, aiming to mitigate excessive cordon queues and prevent spillback. The weight coefficient $\omega_{i,p}(k)$ captures the trade-off between these two objectives, whose calculation method will be presented later.

Eq. (7)-Eq. (10) are the constraints of the Stage I model. Eq. (7) models the queue evolution of lane group (i,p) under the assumption of constant demand over two adjacent control intervals (Yang et al., 2017). Eq. (8) limits the inflow by the minimum and maximum admissible values. Eq. (9) ensures that the inflow does not exceed the downstream capacity, avoiding spillback propagation. Finally, Eq. (10) restricts the sum of inflows across all gated lane groups to be no greater than $u^{ir}(k)$ to prevent network gridlock.

Unlike existing multi-objective formulations where the weights are pre-defined, the proposed PI-Balance model allows $\omega_{i,p}(k)$ to be adjusted dynamically to make the model aware of potential spillback at the perimeter. To determine $\omega_{i,p}(k)$, we first define the *minimum spillback-prevention inflow* for each lane group. A lane group is considered at risk of spillback when its queue length exceeds a threshold, set as a fraction μ of its storage capacity $c_{i,p}$. Accordingly, $\tilde{u}_{i,p}(k)$ is defined as the minimum inflow that keeps the resulting queue below the threshold. In practice, this value is bounded by the inflow limits and downstream capacity. Based on these constraints, $\tilde{u}_{i,p}(k)$ is computed by:

$$\tilde{u}_{i,p}(k) = \min\left[u_{i,p}^{\max}, c_{i,p}^{down} - q_{i,p}^{down}(k), \max\left[u_{i,p}^{\min}, q_{i,p}(k) + a_{i,p}(k)C - \mu \cdot c_{i,p}\right]\right] \quad \forall i \in \mathcal{I}, p \in \mathcal{P}_i^{\text{in}} \tag{11}$$

where max[·] and min[·] denote the maximum and minimum operators, respectively.

The corresponding queue length $\tilde{q}_{i,p}(k)$, which represents the maximum admissible queue length with respect to spillback prevention, can then obtained by:

$$\tilde{q}_{i,p}(k) = q_{i,p}(k) + a_{i,p}C - \tilde{u}_{i,p}(k) \quad \forall i \in \mathcal{I}, p \in \mathcal{P}_i^{\text{in}} \tag{12}$$

We further define $\Delta u(k)$ as the amount by which the sum of $\tilde{u}_{i,p}(k)$ over all gated lane groups exceeds $u^{cr}(k)$. This quantity captures the conflict between network-level efficiency and cordon-level spillback prevention, which is not captured when only network-level control performance is considered. The formula is given by:

$$\Delta u(k) = \sum_{i \in \mathcal{I}} \sum_{p \in \mathcal{P}_i^{\text{in}}} \tilde{u}_{i,p}(k) - u^{cr}(k) \tag{13}$$

Based on the definition of $\tilde{q}_{i,p}(k)$ and $\Delta u(k)$, the weight coefficient $\omega_{i,p}(k)$ is defined as:

$$\omega_{i,p}(k) = \frac{\max[\epsilon, \Delta u(k)]}{\tilde{q}_{i,p}(k)} \quad \forall i \in \mathcal{I}, p \in \mathcal{P}_i^{\text{in}} \tag{14}$$

where ϵ is a small positive constant.

The design of $\omega_{i,p}(k)$ enables the model to simultaneously capture the trade-off between network-level and cordon-level objectives while balancing queue lengths across lane groups. On the one

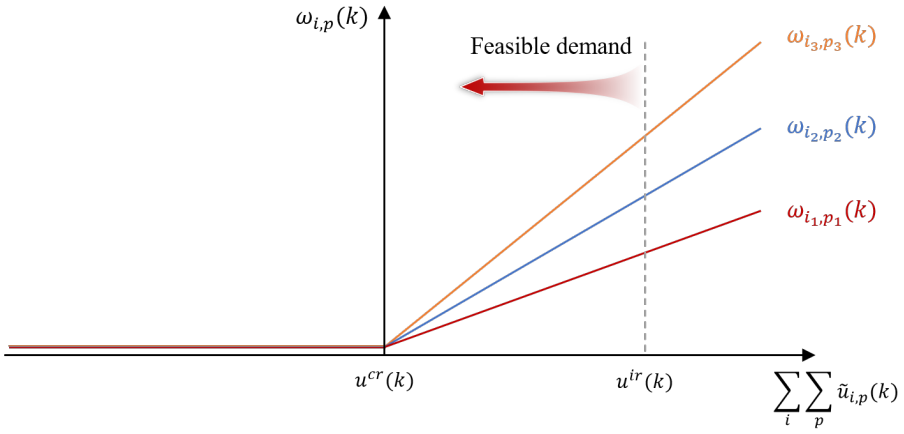


Figure 2: Relationship between $\omega_{i,p}(k)$ and the aggregate spillback-prevention inflow. The three curves correspond to lane groups with different $\tilde{q}_{i,p}(k)$.

hand, the numerator reflects the trade-off through $\Delta u(k)$. When $\Delta u(k) \leq 0$, the spillback-prevention inflow is compatible with the PC requirement, thus a small value is assigned and network efficiency is prioritized; when $\Delta u(k) > 0$, the weight increases with the additional spillback-prevention demand, giving higher priority to the cordon-level objective, as shown in Figure 2. On the other hand, the denominator is introduced to balance queue lengths among gated lane groups. Under the assumption that the gated inflows are independent on each lane group, the first-order condition with respect to $u_{i,p}(k)$ can be calculated by:

$$\frac{\partial J}{\partial u_{i,p}(k)} = 2\left(\sum_{i\in\mathcal{I}}\sum_{p\in\mathcal{P}_i^{\text{in}}} u_{i,p}(k) - u^{cr}(k)\right) - 2\max[\epsilon, \Delta u(k)] \cdot \frac{q_{i,p}(k+1)}{\tilde{q}_{i,p}(k)} \tag{15}$$

In Eq. (15), the last term $q_{i,p}(k+1)/\tilde{q}_{i,p}(k)$ represents the relative queue length of the lane group, while the remaining terms are aggregated across all gated lane groups. As a result, the optimization tends to equalize relative queue lengths across lane groups.

Stage II: Decentralized optimization of perimeter signals

Given the optimal inflow $u_{i,p}(k)$ obtained in Stage I, Stage II determines the signal timing plan of each perimeter intersection to implement the prescribed inflow. Unlike typical isolated intersections, movements at perimeter intersections can be naturally classified into inflow, outflow, and secondary movements (Tsitsokas et al., 2023; Yu et al., 2025). Traffic flows on different types of movements exhibit heterogeneous and time-varying arrival patterns under PC. Existing studies often adjust only the green durations of gated movements, while keeping the phase sequence fixed (He et al., 2024), which is insufficient under such dynamic demand conditions. To address this limitation, a group-based signal control approach is adopted in Stage II, allowing compatible movements to be flexibly combined and their sequence explicitly optimized, so that the signal plan can better adapt to time-varying arrival patterns.

P2:

$$\max_{\mathbf{g},\mathbf{t},\mathbf{\Delta}} J_2 = \sum_{p\in\mathcal{P}_i} \theta_{i,p} o_{i,p} - \alpha \sum_{p\in\mathcal{P}_i^{\text{in}}} (o_{i,p} - u_{i,p})^2 \tag{16}$$

$$\text{subject to} \quad o_{i,p} = \min\left[s_{i,p} * g_{i,p}, q_{i,p} + a_{i,p} * (g_{i,p} + t_{i,p})\right], \qquad \forall p \in \mathcal{P}_i \tag{17}$$

$$o_{i,p} \leq c_{i,p}^{down} - q_{i,p}^{down}, \qquad \forall p \in \mathcal{P}_i \tag{18}$$

$$\delta_{p_1,p_2}^i + \delta_{p_2,p_1}^i = 1, \qquad \forall (p_1,p_2) \in \Psi_i \tag{19}$$

$$t_{i,p_1} + \delta_{p_1,p_2}^i C \geq t_{i,p_2} + g_{i,p_2} + \tau, \qquad \forall (p_1,p_2) \in \Psi_i \tag{20}$$

$$t_{i,p} + g_{i,p} + \tau \leq C, \qquad \forall p \in \mathcal{P}_i \tag{21}$$

$$g^{\min} \leq g_{i,p} \leq g^{\max}, \qquad \forall p \in \mathcal{P}_i \tag{22}$$

where $\theta_{i,p}$ is the weight of the throughput of lane group (i,p); α the parameter that determines the strictness of the soft constraint; $s_{i,p}$ the saturation flow rate (SFR) of lane group (i,p); $t_{i,p}$ and $g_{i,p}$ the green start and green duration of lane group (i,p), respectively; τ the clearance time; $\delta^i_{p_1,p_2}$ the display sequence of two incompatible lane groups (i,p_1) and (i,p_2).

The objective of the Stage II model jointly accounts for local operational efficiency and the PC requirement. The first term maximizes the total weighted throughput of the intersection, thereby improving trip completion, while the second term penalizes the deviation between the realized outflow $o_{i,p}(k)$ and the target inflow $u_{i,p}(k)$ determined in Stage I. The constraints of the model include the calculation of the throughput of each lane group, downstream capacity limits, and feasible phase design requirements (Silcock, 1997).

By solving model **P2** for each intersection, the signal timing plan for the next control interval is obtained, achieving a balance between network-level and cordon-level performance.

3 Results and discussion

Experiment settings

This section evaluates the proposed two-stage framework in the microscopic simulator SUMO (Lopez et al., 2018), with performance examined from both network-level and cordon-level perspectives. A 5×5 grid network is constructed, where the 16 outermost intersections form the perimeter of the PN, as shown in Figure 3.

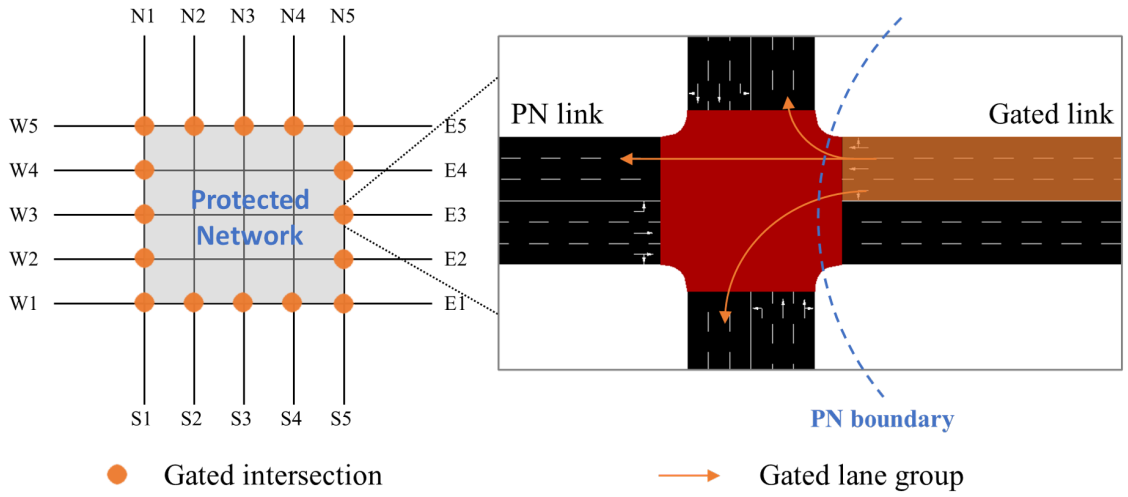
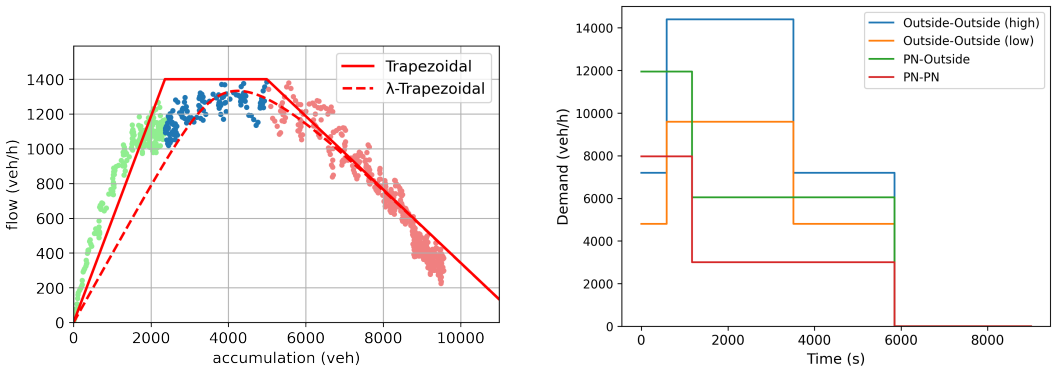


Figure 3: Illustration of the network for case study.

The trapezoidal and λ-trapezoidal MFDs are calibrated using simulation data, from which the critical accumulation N^{cr} and the upper bound of the flat-peak region N^{ub} are identified as approximately 4300 and 5000 vehicles, respectively (see Figure 4(a)). Traffic demand is designed as an unbalanced pattern. Three types of trips are considered: "Outside $\rightarrow$ Outside", "PN $\rightarrow$ Outside", and "PN $\rightarrow$ PN". Specifically, the "Outside $\rightarrow$ Outside" demand generated from the western and northern links is higher than that from the opposite directions, as shown in Figure 4(b).

Benchmark strategies are selected for both stages. For Stage I, we consider the conventional PI feedback perimeter control (Aboudolas & Geroliminis, 2013) and the queue-balancing PI-Cordon method (PIC for short) (Keyvan-Ekbatani et al., 2021), with both N^{cr} and N^{ub} used as set-points (denoted by *Crit* and *Incr* respectively). For Stage II, we compare the group-based model with a rule-based signal timing method proposed in Keyvan-Ekbatani et al. (2019), in which green durations are adjusted according to pre-defined rules while the phase sequence remains fixed.



(a) MFD of the grid network.

(b) Unbalanced demand settings.

Figure 4: Illustration of the MFD of the network and the unbalanced traffic demand.

Evaluation of Stage I model

Detailed results are presented in Table 1. Overall, the PIB model outperforms the benchmark methods. It consistently achieves a lower spillback duration, average vehicle delay, and the standard deviation (Std.) of cordon queue length, showing its effectiveness in mitigating spillback and balancing queues. At the network level, compared with PI (Crit) and PIC (Crit), PIB leads to a slight increase in the total travel time (TTT) within the PN. Nevertheless, the reduction in vehicle delay at the perimeter enables PIB to achieve the lowest TTT of the entire network.

Table 1: Performance of each strategy on primary metrics.

Performance metric	Strategies				
	PI (Crit)	PI (Incr)	PIC (Crit)	PIC (Incr)	**PIB**
Completed trips (veh)	47633	44018	**47665**	46485	**47665**
Spillback duration (s)	2348	2505	1940	1564	**1458**
Average delay (s)	787.97	839.45	787.38	719.03	**687.60**
Std. of cordon queue (m)	268.20	317.85	138.58	162.48	**118.42**
TTT of the network (10^5 s)	701.52	763.76	689.98	717.97	**671.07**
TTT within the PN (10^5 s)	302.08	379.83	**294.93**	366.65	319.36

Figure 5 illustrates the evolution of vehicle accumulation within the PN. From around 2500 s onward, the growth of cordon queues indicates an increasing spillback risk. Correspondingly, the PN accumulation rises from N^{cr} to N^{ub}, reflecting the spillback-aware adjustment of the set-points. It can also be seen that PI (Crit), PIC (Crit), and PIB clear all vehicles, whereas PI (Incr) and PIC (Incr) fail to prevent gridlock and leave some trips unfinished, indicating that N^{ub} is too aggressive for fixed set-point strategies.

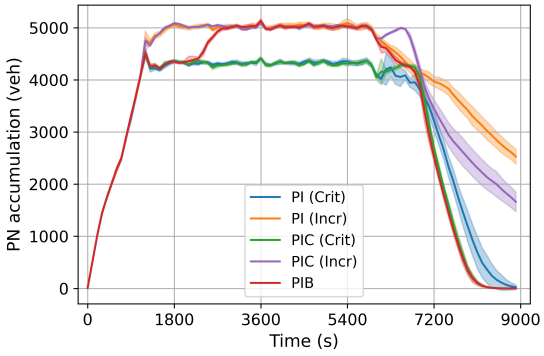
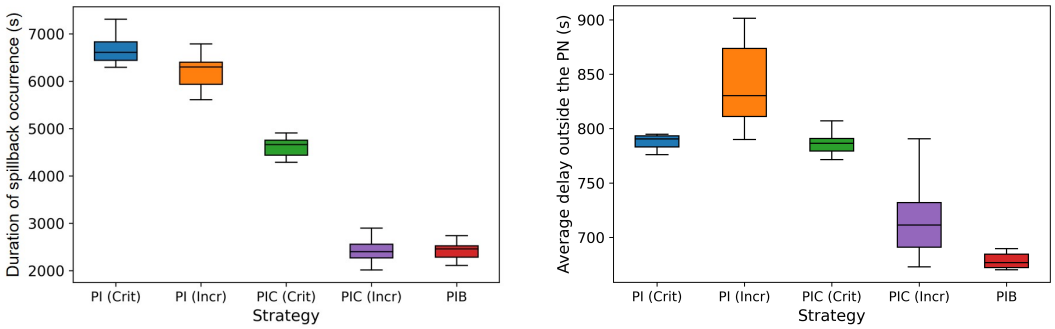


Figure 5: Comparison of vehicle accumulation within the PN.

Figure 6 compares the spillback duration and average vehicle delay at the perimeter. Under unbalanced traffic demand, both queue balancing and set-point adjustment strategies contribute to spillback mitigation. Therefore, PIC (Incr) and PIB show comparable performance on cordon queue management, significantly outperforming the other benchmark strategies. However, PIC (Incr) does not improve average delay because the excessively high set-point may induce network gridlock. The propagation of congestion offsets the gains at the cordon level. In contrast, PIB remains more stable and consistently reduces external delay.

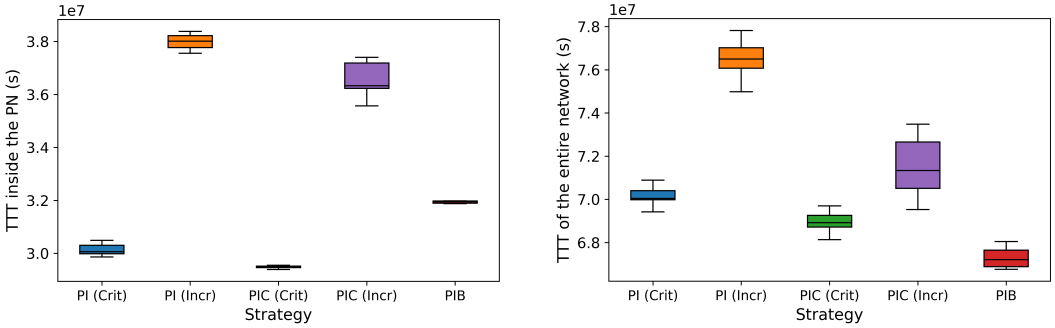


(a) Boxplot of spillback occurrence.

(b) Boxplot of vehicle delay.

Figure 6: Comparison of spillback duration and average delay at the perimeter.

At the network level, PIB leads to a slight increase in total travel time within the PN compared with PI (Crit) and PIC (Crit), due to the increase in accumulation and reduced average speed. However, this increment is offset by the reduction in perimeter delay, resulting in the lower TTT of the entire network, as shown in Figure 7. Moreover, the total travel time under PIC (Incr), which shows comparable performance at the cordon level, is substantially higher due to PN gridlock. In contrast, PIB achieves a better balance between internal efficiency and external congestion management.



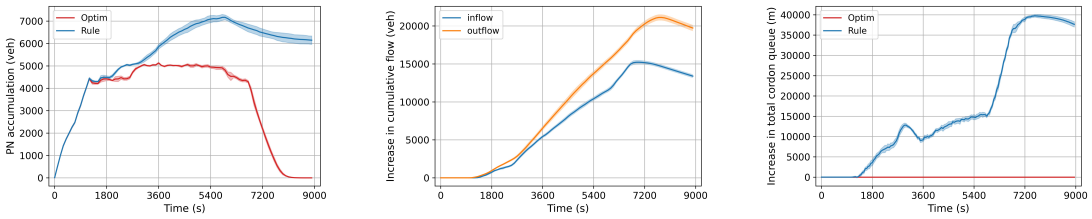
(a) Boxplot of TTT within the PN.

(b) Boxplot of TTT of the entire network.

Figure 7: Comparison of total travel time.

Evaluation of Stage II model

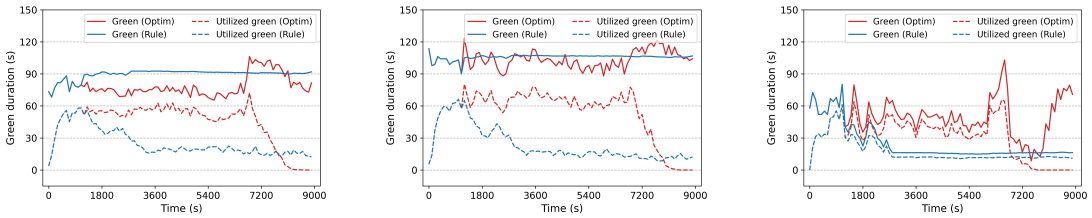
We further illustrate the necessity of the signal timing optimization model developed in Stage II. Figure 8 compares the evolution of vehicle accumulation within the PN, total inflow, and total cordon queue length under the two strategies. It can be observed that the rule-based method leads to an earlier increase in PN accumulation. This is because the outflow of the PN in each control interval is consistently lower during the loading period. As a result, the PI controller computes a lower total gated inflow for subsequent intervals, which accelerates the growth of cordon queues. Consequently, cordon queues reach the threshold value earlier under rule-based method, triggering a premature increase in accumulation. The persistently lower outflow eventually prevents vehicles from leaving the PN in a timely manner, resulting in network gridlock.



(a) Profile of PN accumulation. (b) Increase in cumulative flow. (c) Profile of total queue length.

Figure 8: Comparison of vehicle accumulation and total queue length.

Figure 9 compares the green time for outflow, inflow, and secondary movements, together with the utilized green time within which vehicles are discharged. Although the rule-based strategy assigns longer green durations to outflow movements, the lack of phase combination and sequencing optimization leads to a mismatch with actual demand. As a result, the utilized green time (corresponding to the number of vehicles discharged) is significantly lower than that of the optimization-based approach, explaining the reduced outflow observed in Figure 8. This inefficiency propagates to the Stage I model by reducing the total gated inflow and weakening the overall effectiveness of perimeter control.



(a) Outflow movements (b) Inflow movements (c) Secondary flow movements

Figure 9: Comparison of green / utilized green of different types of movements.

4 Conclusions

This study proposes a two-stage perimeter control framework for signal optimization at perimeter intersections. The concept of buffer capacity is introduced and calibrated based on the λ-trapezoidal MFD. Building on this, Stage I formulates a spillback-aware multi-objective model with dynamically adjusted weights, enabling a real-time trade-off between network-level efficiency and cordon-level queue management. Stage II develops a group-based signal optimization model that jointly determines green durations and phase structures to accommodate time-varying demand and improve local throughput. Simulation results demonstrate the effectiveness of the proposed framework at both levels. At the network level, the model avoids network gridlock and reduces total travel time. At the cordon level, it significantly mitigates spillback and manages to balance cordon queues. In addition, the group-based signal design enhances local efficiency and the effectiveness of perimeter control.

Future research will focus on dynamic calibration of MFD parameters taking into account the effect of control strategies, and extending the framework to network with a dynamic cordon area to better address potential risk of spillback.

Acknowledgements

This work was supported by Financial support from the National Natural Science Foundation of China (No. 52325210, 52302411) and the Shanghai Academic Research Leader Program (No. 23XD1404200).

References

Aboudolas, K., & Geroliminis, N. (2013). Perimeter and boundary flow control in multi-reservoir heterogeneous networks. *Transportation Research Part B: Methodological*, *55*, 265–281.

Ambühl, L., Loder, A., Bliemer, M. C., Menendez, M., & Axhausen, K. W. (2020). A functional form with a physical meaning for the macroscopic fundamental diagram. *Transportation Research Part B: Methodological*, *137*, 119–132.

Chen, C., Huang, Y., Lam, W. H., Pan, T., Hsu, S., Sumalee, A., & Zhong, R. (2022). Data efficient reinforcement learning and adaptive optimal perimeter control of network traffic dynamics. *Transportation Research Part C: Emerging Technologies*, *142*, 103759.

Daganzo, C. F. (2007). Urban gridlock: Macroscopic modeling and mitigation approaches. *Transportation Research Part B: Methodological*, *41*(1), 49–62.

Daganzo, C. F., Lehe, L. J., & Argote-Cabanero, J. (2018). Adaptive offsets for signalized streets. *Transportation research part B: methodological*, *117*, 926–934.

Geroliminis, N., & Daganzo, C. F. (2008). Existence of urban-scale macroscopic fundamental diagrams: Some experimental findings. *Transportation Research Part B: Methodological*, *42*(9), 759–770.

Geroliminis, N., Haddad, J., & Ramezani, M. (2012). Optimal perimeter control for two urban regions with macroscopic fundamental diagrams: A model predictive approach. *IEEE Transactions on Intelligent Transportation Systems*, *14*(1), 348–359.

Haddad, J. (2017). Optimal perimeter control synthesis for two urban regions with aggregate boundary queue dynamics. *Transportation Research Part B: Methodological*, *96*, 1–25.

Hamedmoghadam, H., Zheng, N., Li, D., & Vu, H. L. (2022). Percolation-based dynamic perimeter control for mitigating congestion propagation in urban road networks. *Transportation research part C: emerging technologies*, *145*, 103922.

He, Z., Han, Y., Ji, X., Yu, H., Liu, P., & Kouvelas, A. (2024). Hierarchical perimeter control with network heterogeneity reduction and queue management. *IEEE Intelligent Transportation Systems Magazine*.

Keyvan-Ekbatani, M., Carlson, R. C., Knoop, V. L., & Papageorgiou, M. (2021). Optimizing distribution of metered traffic flow in perimeter control: Queue and delay balancing approaches. *Control Engineering Practice*, *110*, 104762.

Keyvan-Ekbatani, M., Gao, X., Gayah, V. V., & Knoop, V. L. (2019). Traffic-responsive signals combined with perimeter control: investigating the benefits. *Transportmetrica B: Transport Dynamics*, *7*(1), 1402–1425.

Keyvan-Ekbatani, M., Kouvelas, A., Papamichail, I., & Papageorgiou, M. (2012). Exploiting the fundamental diagram of urban networks for feedback-based gating. *Transportation Research Part B: Methodological*, *46*(10), 1393–1403.

Kouvelas, A., Saeedmanesh, M., & Geroliminis, N. (2017). Enhancing model-based feedback perimeter control with data-driven online adaptive optimization. *Transportation Research Part B: Methodological*, *96*, 26–45.

Liu, H., & Gayah, V. V. (2024). N-mp: A network-state-based max pressure algorithm incorporating regional perimeter control. *Transportation Research Part C: Emerging Technologies*, *168*, 104725.

Lopez, P. A., Behrisch, M., Bieker-Walz, L., Erdmann, J., Flötteröd, Y.-P., Hilbrich, R., ... Wießner, E. (2018). Microscopic traffic simulation using sumo. In *2018 21st international conference on intelligent transportation systems (itsc)* (pp. 2575–2582).

Ma, W., Huang, Y., Jin, X., & Zhong, R. (2024). Functional form selection and calibration of macroscopic fundamental diagrams. *Physica A: Statistical Mechanics and its Applications*, *640*, 129691.

Ni, W., & Cassidy, M. J. (2019). Cordon control with spatially-varying metering rates: A reinforcement learning approach. *Transportation Research Part C: Emerging Technologies*, *98*, 358–369.

Silcock, J. (1997). Designing signal-controlled junctions for group-based operation. *Transportation Research Part A: Policy and Practice*, *31*(2), 157–173.

Tsitsokas, D., Kouvelas, A., & Geroliminis, N. (2023). Two-layer adaptive signal control framework for large-scale dynamically-congested networks: Combining efficient max pressure with perimeter control. *Transportation Research Part C: Emerging Technologies*, *152*, 104128.

Yang, K., Zheng, N., & Menendez, M. (2017). Multi-scale perimeter control approach in a connected-vehicle environment. *Transportation research procedia*, *23*, 101–120.

Yu, J., Laharotte, P.-A., Han, Y., Ma, W., & Leclercq, L. (2025). Perimeter control with heterogeneous metering rates for cordon signals: A physics-regularized multi-agent reinforcement learning approach. *Transportation Research Part C: Emerging Technologies*, *171*, 104944.